Inviscid Surface Streamlines and Heat Transfer on Shuttle-Type Configurations

FRED R. DE JARNETTE*
North Carolina State University, Raleigh, N.C.

AND

H. HARRIS HAMILTON†
NASA Langley Research Center, Hampton, Va.

A method is developed which calculates laminar, transitional, and turbulent heating rates on arbitrary blunt-nosed three-dimensional bodies at angle of attack in hypersonic flow. The geometry of the body may be specified analytically, or generated from a doubly cubic spline fit to coordinate points. Inviscid surface streamlines are calculated from Euler's equation using a prescribed pressure distribution. Laminar and turbulent heating rates are determined along a streamline by applying the axisymmetric analog to solutions of the axisymmetric boundary-layer equations. The location of the transition region may be specified optionally by geometric location, momentum thickness Reynolds number, or integrated unit Reynolds number along a streamline. Transitional heating rates are then calculated as a weighted average of the local laminar and turbulent values. Either ideal gas or equilibrium air properties may be used. Results are presented for blunted circular cones, and a typical delta-wing space shuttle orbiter at angle of attack. In comparison with experimental data, the present method was found to yield accurate laminar heating rates and reasonably accurate transitional and turbulent heating rates. The computer program developed to calculate the results presented herein requires only a few seconds of computing time per streamline on the CDC 6600 computer.

Nomenclature

a,b = parameters defined by Eqs. (31) and (32)
B = ratio of principal velocity gradients at stagnation point
$C(\beta),C_1(\beta)$ = parameters used in Eqs. (18) and (23)
D/DS = derivative along a streamline holding β constant
$\hat{e}_T,\hat{e}_{11}$ = unit vectors on body surface, Eqs. (4) and (5)
$\hat{e}_S,\hat{e}_n,\hat{e}_\beta$ = unit vectors in streamline coordinate system, Eqs. (6, 3, and 7)
$\hat{e}_x,\hat{e}_r,\hat{e}_\phi$ = unit vectors in cylindrical doordinate system
f = body radius in Monge's form, $r = f(x,\phi)$
h = scale factor in β-direction, $dq = h\,d\beta$
H = enthalpy, joules/kg
h_S = scale factor in S-direction, $dS = h_S\,d\xi$
L = body length, m
M = Mach number
n = straight-line distance normal to body surface
p = pressure, N/m^2
Pr = Prandtl number
q = distance normal to streamline on body surface, $dq = h\,d\beta$
q_{REF} = heat-transfer rate at stagnation point on a scaled 0.3048-m-radius sphere, w/m^2
q_w = heat-transfer rate at wall, w/m^2
r_N = nose radius, m
$\vec{R}$ = position vector for points on body
$Re_{\infty,L},Re_{\infty,N}$ = freestream Reynolds number based on length and nose radius, respectively.
R_T,R_{11} = principal body radii of curvature at stagnation point
S = distance along a streamline, measured from stagnation point ($dS = h_s\,d\xi$)
S_{11},S_T = body surface coordinates at stagnation point
t = time, sec
t_e = enthalpy ratio, H_e/H_S
U_e,V = velocity at edge of boundary layer, m/sec
$\vec{V}$ = inviscid velocity on surface, m/sec
V_{11},V_T = velocity components along S_{11} and S_T, m/sec
$\hat{V}_\infty$ = unit vector in direction of freestream velocity vector
x,r,ϕ = cylindrical coordinates
x,y,z = Cartesian coordinates
α = angle of attack
β = coordinate normal to streamline on body surface ($dq = h\,d\beta$)
$\bar{\beta}$ = boundary-layer pressure gradient parameter
Γ,δ_ϕ = body angles defined by Eqs. (2) and (1), respectively
ζ_w = wall enthalpy ratio, H_w/H_S
ζ_w' = enthalpy gradient normal to wall
θ = inclination angle of inviscid surface streamline, Eq. (6)
μ = coefficient of viscosity, kg-m/sec
ξ = coordinate along a surface streamline ($dS = h_S\,d\xi$)
ρ = mass density, kg/m^3
σ = angle defined by $\sigma \equiv \phi - \delta_\phi$

Subscripts

e = edge of boundary layer
S = stagnation point
w = wall
∞ = freestream

Introduction

THE calculation of aerodynamic heating on shuttle-type configurations is a challenging problem. Configurations of current interest are three-dimensional (nonaxisymmetric) bodies which operate at large angles of attack during peak heating periods.

Numerical methods have been developed for calculating the inviscid flowfield over three-dimensional bodies at angle of attack.[1,2] However, the application of these techniques to general three-dimensional bodies, typical of space shuttle, will require large computational times. Moreover, no

Presented as Paper 72-703 at the AIAA 5th Fluid and Plasma Dynamics Conference, Boston, Mass., June 26–28, 1972; submitted July 14, 1972; revision received December 7, 1972. Research supported by Contract NAS1-10277, NASA Langley Research Center.

Index categories: Boundary Layers and Convective Heat Transfer—Laminar; Boundary Layers and Convective Heat Transfer—Turbulent.

* Professor of Mechanical and Aerospace Engineering.

† Aerospace Engineer, Aerothermal Branch, Space Systems Division.

general three-dimensional boundary-layer solution exists which can be applied to shuttle-type configurations. This paper presents a relatively simple method for calculating inviscid surface streamlines, and laminar, transitional, and turbulent heating on general three-dimensional bodies at angles of attack. The motivation for this work was to develop an accurate approximation method for making engineering type calculations of three-dimensional heating without requiring a solution of the complete flowfield equations. The basic method is described in detail in Ref. 3, and a description of the computer program is given in Ref. 4. Results presented in this paper are for an ideal gas; however, both ideal gas and equilibrium air properties are included in the present analysis.

Analysis

In order to obtain tractable solutions of three-dimensional flowfields, simplifying approximations are needed for both the inviscid and boundary-layer flows. A substantial simplification to the viscous flow may be achieved through the use of the axisymmetric analog or small cross-flow approximation for three-dimensional boundary layers.[5,6] This approximation allows the heat-transfer rate to be calculated along an inviscid surface streamline by any method applicable to a body of revolution at zero incidence. The distance along the streamline is interpreted as the distance along an equivalent axisymmetric body, and the scale factor or metric coefficient for the surface coordinate normal to the streamline (which is a measure of the streamline divergence) is interpreted as the radius of the equivalent axisymmetric body. Thus, each inviscid streamline corresponds to a different equivalent body or revolution at zero incidence. The axisymmetric analog was shown[7] to be applicable when the ratio of wall to stagnation enthalpy was small, as it is in most space shuttle applications.

Inviscid Surface Streamlines

The major difficulty in applying the axisymmetric analog is the calculation of the inviscid surface streamlines and the corresponding equivalent radius or scale factor. Before describing the technique to calculate these parameters, a method for describing the body geometry must be introduced.

Represent the body geometry by Monge's form $r = f(x,\phi)$ in a cylindrical coordinate system with the unit vectors $\hat{e}_x$, $\hat{e}_r$, and $\hat{e}_\phi$ in the x, r, and ϕ directions, respectively (see Fig. 1). Define the two body angles Γ and δ_ϕ by the relations

$$\tan\delta_\phi = (1/f)(\partial f/\partial\phi) \tag{1}$$

$$\tan\Gamma = \cos\delta_\phi(\partial f/\partial x) \tag{2}$$

where $-\pi/2 \leq \delta_\phi, \Gamma \leq \pi/2$. These two angles are shown in Fig. 2. The unit vector normal to the surface (outer) can be written in terms of Γ and δ_ϕ as

$$\hat{e}_n = -\sin\Gamma\ \hat{e}_x + \cos\Gamma(\cos\delta_\phi\ \hat{e}_r - \sin\delta_\phi\ \hat{e}_\phi) \tag{3}$$

It will also be convenient to define the unit vector ($\hat{e}_T$) tangent to the body in a cross-sectional plane, given by the equation

$$\hat{e}_T \equiv \cos\delta_\phi\ \hat{e}_\phi + \sin\delta_\phi\ \hat{e}_r \tag{4}$$

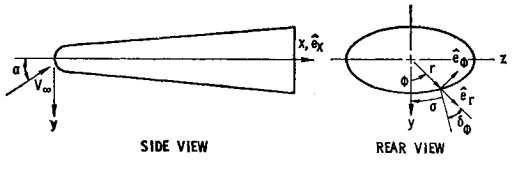

Fig. 1 Body geometry and coordinate system.

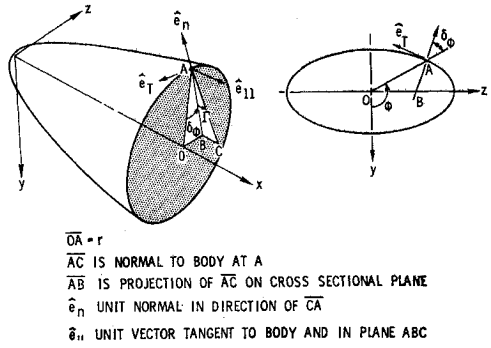

Fig. 2 Geometry of body angles δ_ϕ and Γ.

and the unit vector ($\hat{e}_{11}$) tangent to the surface and perpendicular to $\hat{e}_n$ and $\hat{e}_T$, given by the equation

$$\hat{e}_{11} \equiv \cos\Gamma\ \hat{e}_x + \sin\Gamma(\cos\delta_\phi\ \hat{e}_r - \sin\delta_\phi\ \hat{e}_\phi) \tag{5}$$

Thus $\hat{e}_n$, $\hat{e}_T$, and $\hat{e}_{11}$ are a set of mutually perpendicular unit vectors with $\hat{e}_T$ and $\hat{e}_{11}$ tangent to the body surface. These unit vectors are also shown in Fig. 2.

In order to orient an inviscid surface streamline, let $\hat{e}_S$ be a unit vector in the direction of the streamline with θ the angle between $\hat{e}_S$ and $\hat{e}_{11}$. Then

$$\hat{e}_S = \cos\theta\ \hat{e}_{11} + \sin\theta\ \hat{e}_T \tag{6}$$

Define $\hat{e}_\beta$ as the unit vector tangent to the surface and normal to $\hat{e}_S$,

$$\hat{e}_\beta \equiv -\sin\theta\ \hat{e}_{11} + \cos\theta\ \hat{e}_T \tag{7}$$

Here also $\hat{e}_S$, $\hat{e}_n$, and $\hat{e}_\beta$ are a set of mutually perpendicular unit vectors with $\hat{e}_S$ and $\hat{e}_\beta$ tangent to the surface.

The geometry of the inviscid surface streamlines is determined from Euler's equation

$$D\vec{V}/Dt = -(\nabla p/\rho) \tag{8}$$

where the operator D/Dt is the time derivative along a streamline (for steady flow). In streamline coordinates Euler's equation can be written in the form

$$V\frac{DV}{DS}\hat{e}_S + V^2\frac{D\hat{e}_S}{DS} = -\frac{1}{\rho}\left[\frac{Dp}{DS}\hat{e}_S + \frac{\partial p}{\partial q}\hat{e}_\beta + \frac{\partial p}{\partial n}\hat{e}_n\right] \tag{9}$$

where dq is the differential of arc length in the $\hat{e}_\beta$ direction (normal to the streamline) and DS is the differential of arc length in the $\hat{e}_S$ direction (along the streamline). Taking the scalar product of $\hat{e}_\beta$ with Eq. (9) and defining the angle $\sigma \equiv \phi - \delta_\phi$, (see Fig. 1) the streamline equation is obtained in the form

$$D\theta/DS = -\sin\Gamma\ D\sigma/DS - (1/\rho V^2)\ \partial p/\partial q \tag{10}$$

which can be integrated along a streamline to obtain θ, the local streamline direction. The first term on the right of Eq. (10) depends on the body geometry whereas the second term depends on the surface pressure distribution. However, before this equation can be applied, transformation operators are needed to relate $D\sigma/DS$ and $\partial p/\partial q$ to their respective derivatives in cylindrical coordinates. These operators are developed in Appendix A.

The geometric location of the streamline (x,ϕ) is given by the following differential equations (also developed in Appendix A)

$$Dx/DS = \cos\theta\cos\Gamma \tag{11}$$

and

$$f(D\phi/DS) = \sin\theta\cos\delta_\phi - \cos\theta\sin\delta_\phi\sin\Gamma \tag{12}$$

Thus, Eqs. (10–12) provide three equations to be integrated along a streamline to obtain θ, x, and ϕ, respectively. Equation (10) is indeterminate at the stagnation point but this indeterminacy can be resolved as shown later in the section on the stagnation region streamlines.

Scale Factors

Since the surface streamlines and their corresponding surface orthogonal lines are curvilinear, the scale factors (metric coefficients) play an important role. To illustrate their importance, the differential arc lengths dS and dq are written as

$$dS = h_S\, d\xi \tag{13}$$

$$dq = h\, d\beta \tag{14}$$

where ξ is the coordinate along a streamline, β is the coordinate normal to the streamlines, and h_S and h are their corresponding scale factors (see Fig. 3). The differentials $d\xi$ and $d\beta$ are exact whereas in general dS and dq are not. Since $d\xi$ and $d\beta$ are exact differentials, mixed partial derivatives involving these variables are interchangeable. With this and the assumption that the flow on the surface is isentropic (i.e., inviscid) the following equation can be obtained for the scale factor h (see development in Appendix B)

$$\frac{1}{h}\frac{D^2h}{DS^2} = (M^2-3)\left[\frac{1}{\rho V^2}\frac{\partial p}{\partial q}\right]^2 - \frac{1}{\rho V^2}\frac{\partial^2 p}{\partial q^2} + \frac{\cos^2\Gamma\cos\delta_\phi}{f}\left[\frac{\partial\Gamma}{\partial x}\frac{\partial\sigma}{\partial\phi} - \frac{\partial\sigma}{\partial x}\frac{\partial\Gamma}{\partial\phi}\right] \tag{15}$$

This differential equation can be integrated along a streamline to determine the scale factor or equivalent radius h (see Fig. 3) for use in the axisymmetric analog and the integration can be carried out independent of other streamlines. The term $\partial^2 p/\partial q^2$ can be expressed in terms of derivatives with respect to x and ϕ by repeated use of the transformation operator developed in Appendix A.

The geodesic curvature of the surface lines orthogonal to the streamlines is $1/h\ Dh/DS$, and it is a measure of the amount that the streamlines diverge ($Dh/DS > 0$) or converge ($Dh/DS < 0$). The form of Eq. (15) indicates that h is not completely determinate; it may be multiplied by a constant or any function of β. For the analysis herein the coordinate β is chosen so that it reduces to the circumferential angle ϕ and h reduces to the radius r for the special case of an axisymmetric body at zero incidence.

To summarize, the calculation of an inviscid surface streamline and its corresponding scale factor h is accomplished by numerically integrating Eqs. (10–12, and 15) for θ, x, ϕ, and h, respectively. Initial conditions required to start the integration of each streamline are developed in the section on the stagnation region. To perform the integration, the body geometry and surface pressure distribution must be specified. Two methods have been used to describe the body geometry: 1) analytic equations and 2) a two-dimensional cubic spline function generated from coordinates of points around the periphery of the body at several axial stations.[3] Although in theory the second method can be used to describe very general body shapes, in practice it is limited to nonplanar type bodies. This restriction is necessary to avoid oscillations in the body surface slope that can induce errors in the streamline solution. Further work is needed to generalize the geometry description.

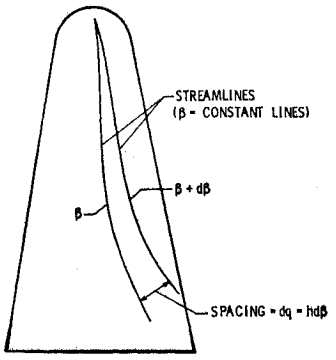

Fig. 3 Scale factor, h.

Stagnation Region Streamlines

The equations developed previously for the inviscid surface streamlines and scale factor h are singular at the stagnation point. Therefore, an analytic solution will be developed for a small region surrounding the stagnation point. This solution will provide the initial conditions to start the numerical integration of the streamline and scale factor differential equations.

For the region surrounding the stagnation point, it is advantageous to use coordinates S_{11} and S_T which are along the body surface and in the directions of the unit vectors $\hat{e}_{11}$ and $\hat{e}_T$, respectively. The coordinate S_{11} is on the body surface along the windward plane of symmetry and S_T is normal to S_{11} on the body surface. It is assumed that the stagnation point coincides with the Newtonian stagnation point. In this region the equation of a streamline may be approximated by the relation

$$DS_T/DS_{11} = V_T/V_{11} \simeq (1/B)(S_T/S_{11}) \tag{16}$$

where

$$B = (\partial V_{11}/\partial S_{11})_S/(\partial V_T/\partial S_T)_S \tag{17}$$

is the ratio of the principal velocity gradients at the stagnation point. Equation (16) may be integrated to yield

$$S_{11} = C(\beta)\, S_T{}^B \tag{18}$$

where the parameter $C(\beta)$ distinguishes one streamline from another because β is constant along a streamline. For convex bodies $B > 0$, and the stagnation point is a nodal point. When the stagnation region is spherical, $B = 1$, and the streamlines emanate radially. Otherwise the slope of the streamlines at the stagnation point $\tan\theta_S$ (where $\tan\theta_S \equiv DS_T/DS_{11}$) is equal to 0 for $0 \leq B < 1$ and ∞ for $B > 1$.

Reshotko[8] has expressed the ratio of velocity gradients at the stagnation point (B) by the equation

$$B = R_T/R_{11} \tag{19}$$

where

$$R_T = [f/(\cos\Gamma\ \partial\sigma/\partial\phi)]_S \tag{20}$$

and

$$R_{11} = -\,[1/(\cos\Gamma\ \partial\Gamma/\partial x)]_S \tag{21}$$

are the principal radii of curvature.

Considering $\beta = \beta(S_{11}, S_T)$ it is shown in Ref. 3 that the scale factor equation may be written as

$$h(\partial\beta/\partial S_T) = \hat{e}_T \cdot \hat{e}_\beta = \cos\theta \tag{22}$$

from which the following equation is obtained[3]

$$h = C_1(\beta)S_{11}/[1 + B^2 S_{11}{}^2/S_T{}^2]^{1/2} \tag{23}$$

The parameter $C_1(\beta)$ is constant along a streamline, but differs from one streamline to another. Equations (18) and (23) provide the initial conditions at some selected point, near the stagnation point, to start the numerical integration of a streamline. The coordinates of this selected point determines $C(\beta)$ from Eq. (18) whereas $C_1(\beta)$ is arbitrary since h is not completely determinant.

Stagnation-Point Heat-Transfer Rate

Previous investigators[6,7,9] have been unable to obtain the correct limiting form of the heating rate at a general three-dimensional stagnation point using the axisymmetric analog because the scale factor h could not be evaluated accurately in this region. However, in the present analysis, the limiting form of the stagnation-point heating rate can be obtained since Eq. (23) gives an accurate expression for h. When the axisymmetric analog is applied to Lees' equation[10] for q_w, the limiting form at the stagnation point is the same as the general three-dimensional stagnation-point heat-transfer rate obtained by Reshotko[8] for a cold wall.‡

Using the axisymmetric analog, the heating rate along an inviscid surface streamline is obtained from an expression for the heating rate on an equivalent axisymmetric body at zero incidence by replacing the body radius by the scale factor h and the distance along the body surface by the distance along the streamline. With these replacements, Lees' equation for a cold wall[10] becomes

$$q_w = \frac{0.5\, Pr^{-0.67}(\rho_e\mu_e V_\infty)^{1/2} H_S (p/p_S)(U_e/V_\infty) h}{(2)^{1/2}\left[\int_0^S \frac{p}{p_S}\frac{U_e}{V_\infty} h^2\, DS\right]^{1/2}} \tag{24}$$

This equation can be applied independently to any inviscid surface streamline on a three-dimensional body; however, it is indeterminate at the stagnation point where $U_e = 0$ and $h = 0$. This indeterminacy can be resolved by using the results obtained for stagnation region streamlines from the previous section, where it can be shown that

$$U_e = V = V_T/\sin\theta = (\partial V_T/\partial S_T)_S\, S_T/\sin\theta \tag{25}$$

$$DS = DS_T/\sin\theta \tag{26}$$

$$\sin\theta = S_T/(B^2 S_{11}{}^2 + S_T{}^2)^{1/2} \tag{27}$$

Then, using the approximation $p/p_S \simeq 1$, the following limit is obtained

$$\lim_{S\to 0} \frac{(p/p_S)(U_e/V_\infty)h}{\left[\int_0^S \frac{p}{p_S}\frac{U_e}{V_\infty} h^2\, DS\right]^{1/2}} = \left[\frac{1}{V_\infty}\left(\frac{\partial V_T}{\partial S_T}\right)_S 2(1+B)\right]^{1/2} \tag{28}$$

When this result is substituted into Eq. (24), the resulting equation is the same as that obtained by Reshotko for a cold wall.

For the present analysis, the three-dimensional stagnation-point heat-transfer rate is calculated by adaptation of the equation given in Ref. 9, but modified so that if reduces to rates compatible with experimental results in the limit of two-dimensional and axisymmetric stagnation points. This yields

$$q_{w,S} = 0.768\left[\frac{B+1}{2}\right]^{1/2}(1.033)\left[\frac{1+0.527\,\bar\beta_S{}^{0.686}}{1.116+0.411\,\bar\beta_S{}^{0.686}}\right] + p_r{}^{-0.6}\left[\frac{\partial V_T}{\partial S_T}\right]_S^{1/2} \times (\rho_w\mu_w)_S{}^a(\rho_e\mu_e)_S{}^b (H_S - H_w) \tag{29}$$

In this equation, the pressure gradient parameter $\bar\beta$ is given by

$$\frac{\bar\beta t_e}{(D/DS)[U_e/V_\infty]} = \frac{2\int_0^S \frac{p}{p_S}\frac{U_e}{V_\infty} h^2\, DS}{[(p/p_S)(U_e/V_\infty)h]^2} \tag{30}$$

and the exponents a and b are assumed to vary linearly with $\bar\beta_S$,

$$a = 0.1 - 0.08\,(\bar\beta_S - 0.5) \tag{31}$$

$$b = 0.5 - a \tag{32}$$

‡ The axisymmetric analog was not used in Reshotko's analysis.

Taking the limit of Eq. (35), it is found that

$$\bar\beta_S = \begin{cases} 1/(B+1) \text{ for } B > 1 \\ B/(B+1) \text{ for } 0 \le B \le 1 \end{cases} \tag{33}$$

Beckwith[6] used $\bar\beta_S \simeq 1 - 0.5B$ for $0.5 \le B \le 1$, which gives the correct values for a sphere ($B = 1$, $\bar\beta_S = 0.5$) and a cylinder ($B = 0$, $\bar\beta_S = 1$), but disagrees with Eq. (33). Equation (33) gives the correct value for a sphere but for the cylinder ($B = 0$) it gives $\bar\beta_S = 0$. This result is not surprising since in the axisymmetric analog the streamlines are assumed to originate from a single stagnation point, and therefore all the streamlines on the cylinder are forced to emanate from this point rather than the stagnation line along a generator of the cylinder.

The velocity gradient used in Eq. (29) is obtained from modified Newtonian theory and is given by the equation

$$\left[\frac{\partial V_T}{\partial S_T}\right]_S = \frac{1}{R_T}\left[\frac{2(p_S - p_\infty)}{\rho_S}\right]^{1/2} \tag{34}$$

Surface Heating Rates

With the streamlines thus determined and the velocity gradients known, the surface heating rates are readily calculated. Application of the axisymmetric analog to solutions of the locally similar boundary-layer equations in Ref. 11 for a relatively cool wall gives the laminar heating-rate ratio $q_w/q_{w,s}$ as

$$\frac{q_w}{q_{w,s}} = \frac{(p/p_S)\,(U_e/V_\infty)\, h\, \zeta_w'/\zeta_{w,s}'}{\left[\frac{2(B+1)}{V_\infty}\left(\frac{\partial V_T}{\partial S_T}\right)_S \int_0^S \frac{p}{p_S}\frac{U_e}{V_\infty} h^2\, DS\right]^{1/2}} \tag{35}$$

where[9]

$$\frac{\zeta_w'}{\zeta_{w,s}'} = \left[\frac{1.116+0.411\,\bar\beta_S{}^{0.686}}{1+0.527\,\bar\beta_S{}^{0.686}}\right]\left[\frac{1+0.527\,\bar\beta^{0.686}}{1.116+0.411\,\bar\beta^{0.686}}\right] + (1.1 - 0.1625\, t_e + 0.0625\, t_e{}^2) \times \frac{(0.85 + 0.15\, t_e - \zeta_w)}{(1-\zeta_{w,s})} \tag{36}$$

Laminar heating rates are obtained by applying Eq. (35) along an inviscid surface streamline, and heating rates along each streamline are computed independently. Solutions are then computed along other streamlines until an adequate surface heating distribution is obtained.

The axisymmetric analog is applicable to turbulent as well as laminar three-dimensional boundary layers.[5] Here the axisymmetric analog is applied to a modified form of the integral method of Reshotko and Tucker[13] to obtain the turbulent momentum thickness. Then the momentum thickness is used to calculate the local skin-friction coefficient from the correlation formula of Spalding and Chi,[14] and finally skin-friction coefficients are converted to turbulent heating rates through Reynolds analogy. Modifications were made in all of these techniques to allow the use of equilibrium air as well as ideal gas properties.

The beginning and end of the transition region is specified by geometric location or some other criterion such as integrated unit Reynolds number or momentum-thickness Reynolds number along a streamline. Then the heating rate in the transition region is calculated as a weighted sum of the local laminar and turbulent heating rates, using the weighting distribution given by Dhawan and Narasimha.[12]

Gas properties at the edge of the boundary layer are calculated from the surface pressure and normal-shock entropy (typical blunt body assumption). For an ideal gas these properties are obtained from standard isentropic relations, whereas for equilibrium air the correlation formulas of Cohen[15] are used in order to keep the computations relatively simple. It should be noted that the assumption of normal-shock entropy is not valid in those regions where the boundary layer has swallowed the entropy layer.

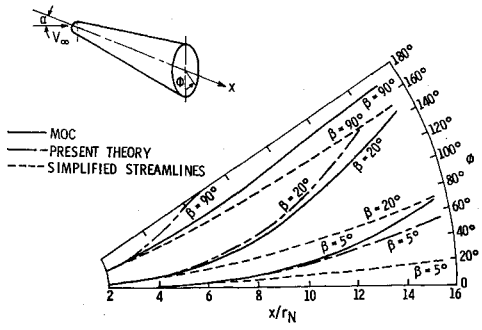

Fig. 4 Surface streamlines on a blunt 9° half-angle cone at $\alpha = 10°$ and $M_\infty = 18$.

Results and Discussion

Inviscid surface streamlines on a blunted 9° half-angle cone are shown for $\alpha = 10°$ and $M_\infty = 18$ in Fig. 4. Each of the streamlines is calculated by three different methods: 1) method of characteristics[16] (MOC), 2) present method using a modified Newtonian pressure distribution, and 3) simplified streamlines[17] (depending only on body geometry). This figure shows that the $\beta = 5°$ and 20° streamlines calculated by the present method using a modified Newtonian pressure distribution are in good agreement with the exact streamlines calculated by the MOC. This is not too surprising since Newtonian theory is known to give a reasonably good prediction of the actual pressure distribution over the windward surface of blunt cones at angle of attack. The $\beta = 90°$ streamline (present method) does not agree well with the result obtained by the MOC, but this is because the Newtonian pressure distribution differs greatly from the MOC pressure distribution on the lee side of the cone. The simplified streamlines for $\beta = 5°$ and 10° differ greatly from the streamlines obtained by the present method and by the MOC. This indicates that in addition to body geometry, the surface pressure distribution has a strong influence on the streamline path. For $\beta = 90°$ the reasonably good agreement of the simplified streamline with the MOC streamline is probably fortuitous.

Figure 5 shows laminar heating rates for a blunt 15° half-angle cone at $\alpha = 20°$, $M_\infty = 10.6$, and $Re_{\infty,N} = 0.0357 \times 10^6$ ($r_N = 0.00925$ m). The experimental data[18] are presented as a ratio of local to stagnation-point heating rates. The figure at the left shows axial distributions of heating-rate ratios for two rays on the cone, the most windward ($\phi = 0°$) and the side ray ($\phi = 90°$). The figure on the right side shows a circumferential distribution of heating at $x/r_N = 26.5$. In computing the heating rates, modified Newtonian pressure distributions were used. Excellent agreement between theory and experiment is obtained.

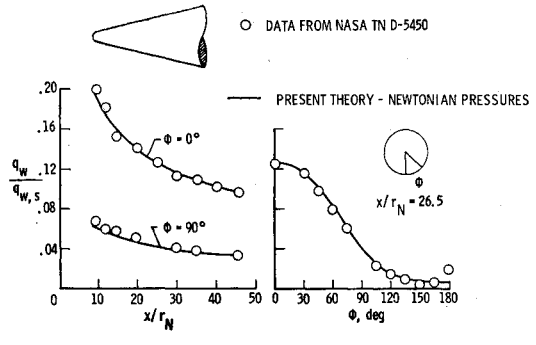

Fig. 5 Heat-transfer distribution on blunt 15° half-angle cone at $\alpha = 20°$, $M = 10.6$, $Re_{\infty,N} = 0.0375 \times 10^6$.

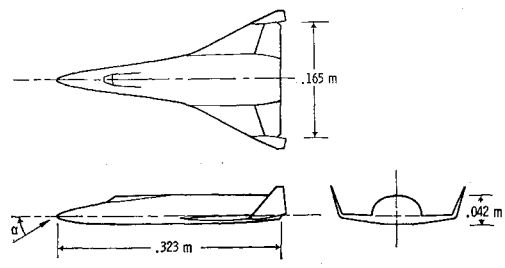

Fig. 6 Typical delta-wing space shuttle orbiter.

Figure 6 shows a typical delta-wing space shuttle orbiter on which computations have been performed. This configuration was selected because of the availability of thermocouple heat-transfer data that were obtained at NASA Ames Research Center[19] (ARC) at $M_\infty = 7.4$. The dimensions shown on the figure are for the ARC thermocouple test model. The surface geometry was described by analytical equations, using a method described in Ref. 2. Basically, it consisted of fitting the planform and plane of symmetry profile with polynomial functions of x, and then using different elliptical segments to fit the upper and lower-half cross sections.

Figure 7 shows a comparison of laminar heating rates computed by the present theory, using a Newtonian pressure distribution, with experimental data at $\alpha = 30°$ for the typical delta-wing orbiter shown in the previous figure. The heat-transfer data are presented as a ratio of local heating rate to a reference value q_w/q_{REF}, where the reference value is at the stagnation point of a scaled 0.3048-m-radius sphere (scale factor = 0.006). Axial distributions of q_w/q_{REF} are presented in the upper left-hand portion of the figure for the windward surface plane of symmetry ($\phi = 0°$). The theory and data are in good agreement over the forward portion of the model (i.e., $x/L < 0.5$) but the theory falls below the data over the aft portion (i.e., $x/L > 0.5$). Newtonian theory predicts a maximum pressure occurring on the windward plane of symmetry for $x/L \leq 0.4$, thus $(\partial^2 p/\partial\phi^2)_{\phi=0} < 0$ in this region and the surface streamlines tend to diverge.§ For $x/L \gtrsim 0.4$ Newtonian theory also predicts a maximum pressure occurring off the windward surface plane of symmetry; thus $(\partial^2 p/\partial\phi^2)_{\phi=0} > 0$ in this region, the surface streamlines tend to converge, and the heating rates are reduced. Examining unpublished experimental pressure data obtained on this same configuration at ARC, one finds that the data (although sparse) tend to indicate that as far back as $x/L = 0.6$, $(\partial^2 p/\partial\phi^2)_{\phi=0} \leq 0$. Thus, the previous calculation was repeated with the condition $(\partial^2 p/\partial\phi^2)_{\phi=0} = 0$ for $x/L = 0.4$ resulting in the heat-transfer

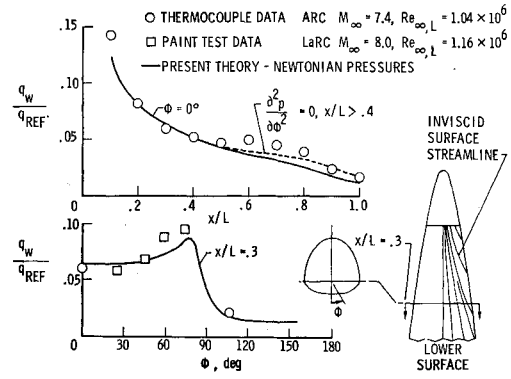

Fig. 7 Heat-transfer distributions and streamline patterns on typical delta-wing orbiter at $\alpha = 30°$.

§ Note $(\partial p/\partial\phi)_{\phi=0} = (\partial^2 p/\partial x\,\partial\phi)_{\phi=0} = 0$ due to symmetry.

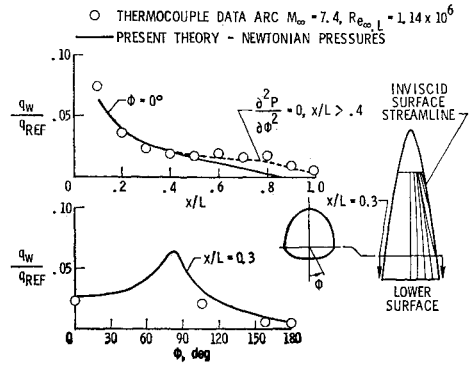

Fig. 8 Heat-transfer distributions and streamline patterns on typical delta-wing orbiter at $\alpha = 15°$.

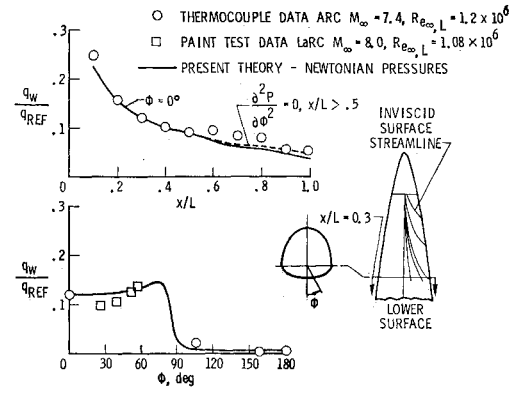

Fig. 9 Heat-transfer distributions and streamline patterns on typical delta-wing orbiter at $\alpha = 53°$.

rates shown by the dashed line. This result is in better agreement with the experimental data suggesting that the previous computation (solid line) underpredicted the data over the rearward portion of the model because of the unrealistic lateral pressure distribution obtained from Newtonian theory.

The circumferential distribution of heating is shown in the lower left-hand portion of the figure. The thermocouple data were supplemented by paint test data obtained at Langley Research Center (LaRC) at $M_\infty = 8$. The theory and data are in reasonably good agreement. In the lower right-hand portion of the figure, the computed inviscid surface streamlines are shown over the forward portion of the lower surface. The streamline divergence increases as the leading edge is approached which accounts for the increase in heating in the vicinity of the leading edge.

Figure 8 shows laminar heating rates and streamline patterns for the same delta-wing orbiter used in the previous figure except that here $\alpha = 15°$. Again, the heating rates using a modified Newtonian pressure distribution (solid line) along the windward plane of symmetry fell below the data over the aft portion. For $x/L \gtrsim 0.15$ it was also found that modified Newtonian theory predicted $(\partial^2 p/\partial \phi^2)_{\phi=0} > 0$ which caused the streamline to converge and finally cross ($h = 0$) at $x/L = 0.85$, driving the heating rate to zero. The results given in Ref. 2 indicate that the transverse pressure distribution is nearly flat across the bottom for $x/L = 0.57$. Therefore, the heating-rate calculations were repeated with $(\partial^2 p/\partial \phi^2)_{\phi=0} = 0$ for $x/L > 0.4$, resulting in the heat-transfer rate shown by the dashed line. This more realistic pressure distribution resulted in heating-rate calculations very close to the experimental data. The circumferential heating-rate distribution at $x/L = 0.3$ is shown in the lower left-hand side of the figure but only one experimental point on the windward side is available for comparison. Stream-line patterns are shown in the lower right-hand side of the figure, and they are in qualitative agreement with those computed in Ref. 20.

Figure 9 shows results similar to those of the previous two figures except the angle of attack is 53°. As in the previous two cases, the modified Newtonian pressures predicted $(\partial^2 p/\partial \phi^2)_{\phi=0} > 0$ for $x/L \gtrsim 0.5$. At this angle of attack it is felt that $(\partial^2 p/\partial \phi^2)_{\phi=0}$ would always be less than or equal to zero; thus this computation was repeated with $(\partial^2 p/\partial \phi^2)_{\phi=0} = 0$ for $x/L > 0.5$ with the results given by the dashed line. The circumferential heating rate compared reasonably well with experiment, and the streamline patterns show the large divergence expected at this large angle of attack.

Laminar, transitional, and turbulent heating rates along the windward surface plane of symmetry of the delta wing orbiter at $\alpha = 30°$ are shown in Fig. 10. Transition was specified by geometric location ($0.55 < x/L < 0.8$). The theory in the laminar region is quite good; however, the theory is significantly lower than the experiment in the transition region. At the end of the body the turbulent theory approaches the experimental results. The large difference at $x/L = 0.7$ and 0.8 may be due to disturbances from the wing-body juncture affecting the experimental data. More comparisons with other turbulent data are needed to access the accuracy of the method of calculating turbulent heating.

Concluding Remarks

A relatively simple method has been developed for computing the three-dimensional heating on shuttle-type configurations. The method is very fast; for example, typical results presented in this paper for a single streamline required only a few seconds of computing time on the CDC-6600 computer. In general, it requires that the surface pressure distribution be obtained independently. For cases where the surface pressure distribution can be approximated with reasonable accuracy, the heating rates computed by the present method have been shown to compare favorably with experimental data. As more exact methods become available for computing the surface pressure distribution, these methods can be used to obtain the surface pressure distributions needed in the present theory. Some further work is needed to include variable entropy at the edge of the boundary layer in the analysis and to improve the mathematical representation of complex geometries.

Appendix A: Development of Transformation Operators

Let $\vec{R}$ be the position vector of any point on the body surface relative to the origin of the cylindrical coordinate system. Then

$$\vec{R} = x\hat{e}_x + f\hat{e}_r$$

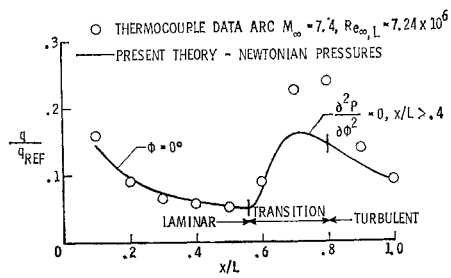

Fig. 10 Laminar, transitional, and turbulent heat-transfer distribution on typical delta-wing orbiter at $\alpha = 30°$.

and

$$d\vec{R}=\left[\hat{e}_x+\frac{\partial f}{\partial x}\hat{e}_r\right]dx+[\hat{e}_\phi+(1/f)(\partial f/\partial\phi)\hat{e}_r]\,f(d\phi) \quad \text{(A1)}$$

On the other hand, $\vec{R}$ can also be considered as a function of the streamline coordinates S and q, hence

$$d\vec{R}=\frac{\partial\vec{R}}{\partial S}dS+\frac{\partial\vec{R}}{\partial q}dq=\hat{e}_S dS+\hat{e}_\beta dq \quad \text{(A2)}$$

Now, equating the right sides of Eqs. (A1) and (A2), the following derivatives can be obtained using Eqs. (4–7).

$$Dx/DS=\hat{e}_x\cdot\hat{e}_S=\cos\theta\cos\Gamma \quad \text{(A3)}$$

$$f(D\phi/DS)=\hat{e}_\phi\cdot\hat{e}_S=\sin\theta\cos\delta_\phi-\cos\theta\sin\delta_\phi\sin\Gamma \quad \text{(A4)}$$

$$\partial x/\partial q=\hat{e}_x\cdot\hat{e}_\beta=-\sin\theta\cos\Gamma \quad \text{(A5)}$$

$$f\,\partial\phi/\partial q=\hat{e}_\phi\cdot\hat{e}_\beta=\cos\theta\cos\delta_\phi+\sin\theta\sin\delta_\phi\sin\Gamma \quad \text{(A6)}$$

Note here that Eqs. (A3) and (A4) are the same as Eqs. (11) and (12) and are used to determine the geometric location (x,ϕ) of the inviscid surface streamline. The derivatives with respect to S and q can be related to derivatives with respect to x and ϕ by the following operators

$$D/DS=(Dx/DS)\,\partial/\partial x+(D\phi/DS)\,\partial/\partial\phi \quad \text{(A7)}$$

$$\partial/\partial q=(\partial x/\partial q)\,\partial/\partial x+(\partial\phi/\partial q)\,\partial/\partial\phi \quad \text{(A8)}$$

Thus, the transformation operators defined by Eqs. (A7) and (A8) along with Eqs. (A3–A6) are used to relate derivatives in streamline coordinates to their respective derivatives in cylindrical coordinates. It should be noted that in the above operators it is implied that all derivatives are evaluated on the body surface where $r=f(x,\phi)$ and $n=0$, thus

$$\partial/\partial x\equiv(\partial/\partial x)_{\phi,n}\text{ and }\partial/\partial\phi=(\partial/\partial\phi)_{x,n}$$

Appendix B: Development of Differential Equation for Equivalent Radius

Since $d\xi$ and $d\beta$ are exact differentials, mixed partial derivatives involving these variables are interchangeable. Thus

$$\partial^2\vec{R}/\partial\xi\partial\beta\equiv\partial^2\vec{R}/\partial\beta\partial\xi \quad \text{(B1)}$$

whereas it is noted that

$$\partial^2\vec{R}/\partial S\partial q\neq\partial^2\vec{R}/\partial q\partial S$$

Now from Eq. (A2) the following two equations can be obtained by differentiation

$$\partial^2\vec{R}/\partial\xi\partial\beta=\partial/\partial\xi(h\,\partial\vec{R}/\partial q)=\partial/\partial\xi(h\hat{e}_\beta)$$

and

$$\partial^2\vec{R}/\partial\beta\partial\xi=\partial/\partial\beta(h_S\,D\vec{R}/DS)=\partial/\partial\beta(h_S\hat{e}_S)$$

Substituting these two equations into Eq. (B1) the following is obtained

$$(\partial h/\partial\xi)\hat{e}_\beta+h\,\partial\hat{e}_\beta/\partial\xi=(\partial h_S/\partial\beta)\hat{e}_S+h_S\,\partial\hat{e}_S/\partial\beta \quad \text{(B2)}$$

The scalar product of $\hat{e}_\beta$ with the preceding equation yields

$$Dh/DS=\partial\theta/\partial\xi+\sin\Gamma\,\partial\sigma/\partial\beta \quad \text{(B3)}$$

This equation cannot be used to calculate the scale factor h along a streamline because $\partial\theta/\partial\beta$ is not known a priori from the solution of Eq. (10).¶ In order to obtain an equation for h, rewrite Eq. (10) in the form

$$-(h_S/\partial V^2)(\partial p/\partial q)=\partial\theta/\partial\xi+\sin\Gamma\,\partial\sigma/\partial\xi \quad \text{(B4)}$$

Differentiating this equation with respect to β and subtracting the result from that obtained by differentiating Eq. (B3) with respect to ξ, the following equation is obtained

$$\frac{1}{h}\frac{D^2h}{DS^2}=-\frac{1}{h_S}\frac{\partial}{\partial q}\left[\frac{h_S}{\rho V^2}\frac{\partial p}{\partial q}\right]+\cos\Gamma\left[\frac{D\Gamma}{DS}\frac{\partial\sigma}{\partial q}-\frac{D\sigma}{DS}\frac{\partial\Gamma}{\partial q}\right] \quad \text{(B5)}$$

Comparing the scalar product of $\hat{e}_S$ with Eq. (B2) with Eq. (B4) it may be seen that

$$(1/h_S)\,\partial h_S/\partial q=(1/\rho V^2)\,\partial p/\partial q \quad \text{(B6)}$$

Finally, using Eq. (B6), the assumption of isentropic flow (i.e., inviscid) on the surface, and the transformation operators developed in Appendix A, Eq. (B5) can be written in the form

$$\frac{1}{h}\frac{D^2h}{DS^2}=(M^2-3)\left[\frac{1}{\rho V^2}\frac{\partial p}{\partial q}\right]^2-\frac{1}{\rho V^2}\frac{\partial^2 p}{\partial q^2}+\frac{\cos^2\Gamma\cos\delta_\phi}{f}\left[\frac{\partial\Gamma}{\partial x}\frac{\partial\sigma}{\partial\phi}-\frac{\partial\sigma}{\partial x}\frac{\partial\Gamma}{\partial\phi}\right] \quad \text{(B7)}$$

This equation is the same as Eq. (15) and can be integrated along a streamline to determine the scale factor or equivalent radius h.

It can be shown that Eqs. (B3) and (B4) are the same as the Mainardi-Codazzi relations[21] and Eq. (B6) is equivalent to the Gauss Characteristic equation.[21]

References

[1] Moretti, G., Grossman, B., and Marconi, F., Jr., "A Complete Numerical Technique for the Calculation of Three-Dimensional Inviscid Supersonic Flow," AIAA Paper 72-192, San Diego, Calif., 1972.

[2] Rakich, J. V. and Kutler, P., "Comparison of Characteristics and Shock Capturing Methods with Application to the Space Shuttle Vehicle," AIAA Paper 72-191, San Diego, Calif., 1972.

[3] DeJarnette, F. R., "Calculation of Inviscid Surface Streamlines and Heat Transfer on Shuttle Type Configurations, Part I.—Description of Basic Method," CR-111921, Sept. 1971, NASA.

[4] DeJarnette, F. R. and Jones, M. H., "Calculation of Inviscid Surface Streamlines and Heat Transfer on Shuttle Type Configurations, Part II.—Description of Computer Program," CR-111922, Sept. 1971, NASA.

[5] Cooke, J. C. and Hall, M. G., "Boundary Layers in Three Dimensions," Rept. Aero. 2635, Feb. 1960, Royal Aircraft Establishment, Farnborough, Hants, England.

[6] Beckwith, I. E., "Similarity Solutions for Small Cross Flows in Laminar Compressible Boundary Layers," TR R-107, 1961, NASA.

[7] Vaglio-Laurin, R., "Laminar Heat Transfer on Three-Dimensional Blunt-Nosed Bodies in Hypersonic Flow," *Jet Propulsion*, Vol. 29, No. 2, Feb. 1959, pp. 123–129.

[8] Reshotko, E., "Heat Transfer to a General Three-Dimensional Stagnation Point," *Jet Propulsion*, Vol. 28, No. 1, Jan. 1958, pp. 58–60.

[9] Cohen, N. B., "Boundary-Layer Similar Solutions and Correlation Equations for Laminar Heat-Transfer Distribution in Equilibrium Air at Velocities Up to 41,100 Feet Per Second," TR R-118, 1961, NASA.

[10] Lees, L., "Laminar Heat Transfer Over Blunt-Nosed Bodies at Hypersonic Flight Speeds," *Jet Propulsion*, Vol. 26, No. 4, April 1956, pp. 259–269, 274.

¶ For those special cases where θ is known, Eq. (B3) can be integrated to yield h by noting that $\partial/\partial\beta\equiv h\,\partial/\partial q$ and using Eq. (A8) to transform the operator.

[11] Beckwith, I. E. and Cohen, N. B., "Application of Similar Solutions to Calculation of Laminar Heat Transfer on Bodies With Yaw and Large Adverse Pressure Gradient in High-Speed Flow," TN D-625, 1961, NASA.

[12] Dhawan, S. and Narasimha, R., "Some Properties of Boundary Layer Flow During the Transition From Laminar to Turbulent Motion," *Journal of Fluid Mechanics*, Vol. 3, No. 4, April 1958, pp. 418–436.

[13] Reshotko, E. and Tucker, M., "Approximate Calculation of the Compressible Turbulent Boundary Layer With Heat Transfer and Arbitrary Pressure Gradient," TN 4154, 1957, NASA.

[14] Spalding, D. B. and Chi, S. W., "The Drag of a Compressible Turbulent Boundary Layer on a Smooth Flat Plate With an Without Heat Transfer," *Journal of Fluid Mechanics*, Vol. 18, Pt. 1, Jan. 1964, pp. 117–143.

[15] Cohen, N. B., "Correlation Formulas and Tables of Density and Some Transport Properties of Equilibrium Dissociating Air for Use in Solutions of the Boundary Layer Equations," TN D-194, 1960, NASA.

[16] Knox, E. C. and Lewis, C. H., "A Comparison of Experimental and Theoretically Predicted Pressure Distributions and Force and Stability Coefficients for a Spherically Blunted Cone at $M_\infty = 18$ and Angle of Attack," TR-65-234, Feb. 1966, Arnold Engineering Development Center, Arnold Air Force Station, Tenn.

[17] DeJarnette, F. R. and Davis, R. M., "A Simplified Method for Calculating Laminar Heat Transfer Over Bodies at an Angle of Attack," TN D-4720, 1968, NASA.

[18] Cleary, J. W., "Effects of Angle of Attack and Bluntness on Laminar Heating-Rate Distributions of a 15° Cone at a Mach Number of 10.6," TN D-5450, 1969, NASA.

[19] Lockman, K. and DeRose, C. E., "Aerodynamic Heating of a Space Shuttle Delta-Wing Orbiter," TM X-62057, 1971, NASA.

[20] Kutler, P., Lomax, H., and Warming, R. F., "Computation of Space Shuttle Flow Fields Using Noncentered Finite-Difference Schemes," AIAA Paper 72-193, San Diego, Calif., 1972.

[21] Weatherburn, C. E., *Differential Geometry of Three Dimensions*, Vol. 1, Cambridge University Press, Cambridge, England, 1931.